Reaction kinetics and mechanism of $BaPbO_3$ formation

M.C. Chang[a,*], J.M. Wu[a], S.Y. Cheng[b], S.Y. Chen[c]

[a] *Department of Materials Science and Engineering, National Tsing Hua University, Hsinchu, Taiwan*
[b] *Materials Research Laboratories, Industrial Technology Research Institute, Chutung, Hsinchu, Taiwan*
[c] *Department of Materials Science and Engineering, National Chiao Tung University, Hsinchu, Taiwan*

Abstract

The influence of starting materials on the formation of $BaPbO_3$ is studied. The reaction kinetics of perovskite $BaPbO_3$ phase formation depends greatly on the phase of lead oxide raw materials. Kinetics of $BaPbO_3$ formation is analyzed by the Johnson–Mehl–Avrami model. The experimental results reveals that the reaction of $BaCO_3$–PbO_2 raw materials has a reaction order of $n=5/2$, and the reaction is controlled by diffusion. On the other hand, in the case of $BaCO_3$–PbO system, the reaction order n is equal to 1. The formation is controlled by the interface reaction. In the final stage of both systems, the reaction orders are the same of about 0.5. The phases left in the final stage are $BaPbO_3$ and $BaCO_3$. © 2000 Elsevier Science S.A. All rights reserved.

Keywords: $BaPbO_3$; Kinetics; Perovskite; Johnson–Mehl–Avrami model

1. Introduction

The crystal structure of $BaPbO_3$ is pseudocubic perovskite at room temperature. Each cell unit contains one $BaPbO_3$ [1]. The perovskite $BaPbO_3$ is a well-known metallic conducting oxide [1]. Due to its structure and high electronic conductivity, $BaPbO_3$ was used as a substrate for the deposition of $Pb(Ni_{1/3}Nb_{2/3})O_3$ thin film by sol–gel techniques [2]. The use of $BaPbO_3$ as substrates is to provide not only the stable formation of perovskite-type $Pb(Ni_{1/3}Nb_{2/3})O_3$, but also high electronic conductivity of $BaPbO_3$ as electrode. This approach is expected to be effective in the development of other perovskite-type thin films, such as $Pb(Zr,Ti)O_3$, $(Ba,Sr)TiO_3$ and $Pb(Mn,Nb)O_3$. In the past, extensive experimental and theoretical investigations had been devoted to $BaPb_{1-x}Bi_xO_3$, since the discovery of superconductivity in the composition range $0.05 \leq x \leq 0.30$, with a maximum T_c of 12 K [3–6]. This superconducting oxide system attracts great interest because of potential applications. One application is as stable Josephson junctions [7], another is application in new cryoelectronic devices [8–10]. However, studies of $BaPbO_3$ formation are relatively rare. Understanding the reaction kinetics and mechanism of $BaPbO_3$ formation is of great help in fabricating $BaPbO_3$ ceramics for the applica-

tion in thick film resistor and preparing the sputtering target for the thin film processing.

In our studies, we found that the formation of $BaPbO_3$ depends greatly on the starting raw materials of lead oxides. There are two simple lead oxide forms: PbO and PbO_2, where lead is di-valent and tetra-valent, respectively. A number of intermediate oxides also exist in which both oxidation states are present together. Lead monoxide occurs in two polymorphic forms. The tetragonal form, litharge, is stable up to 489°C, the orthorhombic form, massicot, is stable above this temperature. Fig. 1 illustrates the crystal structure of litharge. The unit cell contains two PbO groups [11–13]. Massicot is metastable at room temperature [14] and transforms readily to litharge by mechanical forces [15,16], although the additions of small impurities can stabilize the massicot form and prevent its transformation to litharge at room temperature [17].

Lead dioxide is a brownish black crystalline powder which decomposes rather easily into lower oxides and oxygen. Lead dioxide has two crystal forms. The common form, β-PbO_2, the mineral plattnerite, has the rutile structure which is shown in Fig. 2. The orthorhombic dioxide, α-PbO_2, has the columbite structure, which is essentially a hexagonal close-packed assembly of oxygen ions in which one-half of the octahedral holes are occupied by lead ions. The composition of alpha and beta lead dioxide is not always stoichiometric. Density studies indicate that non-stoichiometric compositions result from the presence of
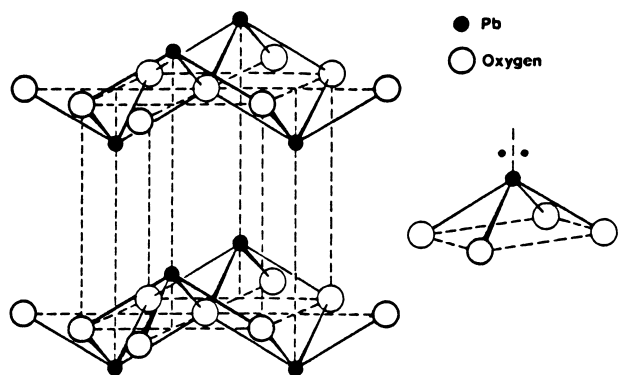
Fig. 1. Crystal structure of litharge.

vacancies in the crystal structure, probably in the ratio of four missing oxygen atoms to one of lead.

In the present investigation, we will report the reaction kinetics and mechanisms of $BaPbO_3$ formation with different raw material systems including $BaCO_3$–PbO and $BaCO_3$–PbO_2.

2. Experimental procedures

The characteristics of the raw materials, consisting of PbO, PbO_2 and $BaCO_3$, are given in Table 1. The powders of $BaCO_3$–PbO and $BaCO_3$–PbO_2 with a composition equivalent to $BaPbO_3$ were ball-milled in a polyethylene jar with ZrO_2 as the grinding media and alcohol solvent as the mixing agent for 20 h. After mixing and drying, samples of 0.1 g powder mixture were extracted from the 200 g batch and were subjected to heat treatment at 600–750°C for 1 min to 3 h in Pt crucibles. Each datum appearing on the heat treatment temperature–time curves was the average of three test results. To reduce the influence of the heating and cooling periods of the heat treatment, the powder mixture samples were put directly into a furnace kept at the preset temperatures. The temperature was measured with a Pt-Pt10Rh thermocouple in contact with the Pt crucible. The time was measured from the instant the powder samples reached the heat treatment temperature, which was generally of the or-
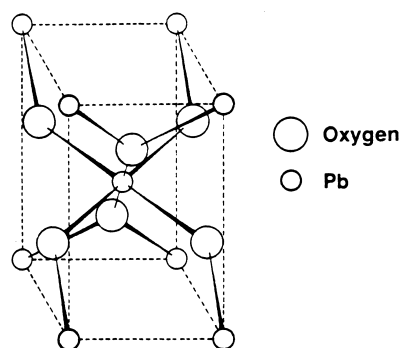

Fig. 2. Crystal structure of plattnerite.

der of 1 min. The samples were pulled out immediately after heat treatment and air-quenched.

The relative amount of the $BaPbO_3$ perovskite phase was determined by the integrated intensities of the (1 1 0) peak of the perovskite phase, the (1 0 1) peak of the litharge and the (1 1 1) peaks of the massicot and the $BaCO_3$ from X-ray powder diffraction (XRD) [1] patterns of heat treated samples, as described by Klug and Alexander [18]. The percentage of formed $BaPbO_3$ perovskite phase was calculated by the following equation:

$$\% \text{ perovskite} = 100 \times \frac{I_{pero}}{\sum I_i} \quad (i = \text{appearing phases})$$

where I_{pero} and I_i represent the integrated intensities of peaks for perovskite and appearing phases, respectively. Differential thermal analysis/Thermogravimetry [2] of the $BaCO_3$–PbO and $BaCO_3$–PbO_2 mixture was conducted from 25 to 1100°C. The heating rate was 5°C min^{-1}. To identify the peaks occurred in DTA analysis, powders heat treated to temperatures lower than the peak temperatures were characterized by XRD.

3. Results and discussion

3.1. DTA and TG analyses

Both DTA/TG data of $BaCO_3$–PbO and $BaCO_3$–PbO_2 are shown in Fig. 3. In $BaCO_3$–PbO system (Fig. 3(a)), decomposition of $BaCO_3$ starts at temperature about 800°C where weight loss increases obviously. Endothermic peaks are found at 798 and 847°C. To prevent the peak occurring at 847°C, DTA was conducted from 25 to 825°C. The powder put in the DTA crucible was identified by XRD after DTA finished the run at 825°C. The diffraction pattern is shown in Fig. 4(a). Not only the product phase ($BaPbO_3$) but also the raw materials (PbO and $BaCO_3$) were found in that powder. The sample was obviously divided into two parts in color: the upper part was black and the lower part was yellow. When DTA was conducted above 850°C, only black color appeared and pure $BaPbO_3$ was formed which is identified by XRD analysis (Fig. 4(b)). Endothermic peaks found at 798 and 847°C are resulted from the formation of $BaPbO_3$ phase. The double peaks are considered to be the effect of rod-shape Al_2O_3 crucible of DTA, which derives 798°C peak for upper part and 847°C peak from lower part reaction. Because lead ion needs to be oxidized more in the formation of $BaPbO_3$, the upper part of crucible is liable to get oxygen from air and presents reaction peak at lower temperature.

In $BaCO_3$–PbO_2 system (Fig. 3(b)), reaction is quite similar to that of $BaCO_3$–PbO system when temperature is higher than 700°C. However, the weight loss starts from lower temperature of 350°C, which is considered to be

Table 1
Characteristic properties of raw materials

Powder	Purity (%)	Particle size (μm)	Phase	Maker
PbO	99.89	7.5	Litharge	Mitsui Lot No. 30520
PbO$_2$	>99	4.2	Plattnerite	Merck Art. 7406
BaCO$_3$	>99	1.8	Witherite	Merck Art. 1714

the decomposition point of PbO$_2$. According to Fig. 3(b), PbO$_2$ is gradually decomposed from 350 to 600°C. Phase change in this temperature range is identified by X-ray powder diffraction. PbO$_2$ phase finally changes into PbO
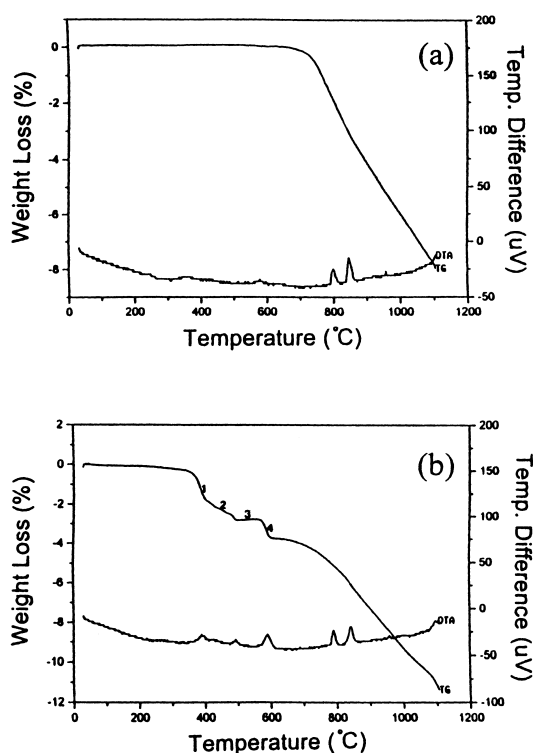

Fig. 3. DTA/TG curves of: (a) BaCO$_3$–PbO powder and (b) BaCO$_3$–PbO$_2$ powder.
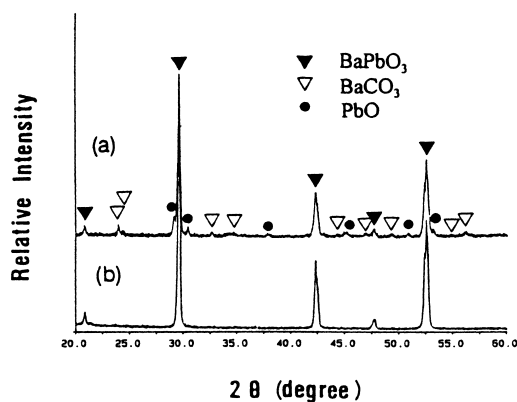

Fig. 4. XRD results of the BaCO$_3$–PbO powder mixtures which were heated in DTA and stop: (a) at 825°C and (b) above 850°C.

phase through PbO$_{1.57}$ and Pb$_3$O$_4$ intermediate phases. The corresponding weight loss of phase change was calculated and shown in Table 2 which confirms the phase change sequence. Weigh loss continues to increase at temperature higher than 600°C. The BaPbO$_3$ phase is formed at temperatures of 780 and 831°C. This behavior is the same as that of BaCO$_3$–PbO system. However, formation temperature of BaPbO$_3$ phase in BaCO$_3$–PbO$_2$ system is a little lower than that in BaCO$_3$–PbO system. It indicates that reaction mechanism may be different for these two systems. Since PbO$_2$ phase has decomposed to PbO before reacting with BaCO$_3$, the PbO phase should play a main role in the formation of BaPbO$_3$ phase. The only difference one can see from Fig. 3 is that the formation temperature of BaPbO$_3$ phase in BaCO$_3$–PbO$_2$ system is lower. It implies that the reaction rate is a little fast in BaCO$_3$–PbO$_2$ system.

3.2. Reaction kinetics of BaPbO$_3$ formation

The formed BaPbO$_3$ phase percentage under isothermal heat treatment is shown in Fig. 5. The duration of 0 means sample is withdrawn directly from oven when the temperature reaches set value. In BaCO$_3$–PbO system, BaPbO$_3$ phase gets 80% at 600°C/60 min, 97% at 700°C/20 min and higher than 97% for 750°C/10 min (Fig. 5(a)). The formation rate is faster in BaCO$_3$–PbO$_2$ system as shown in Fig. 5(b). It took only a few minutes to obtain complete formation of BaPbO$_3$ phase at temperature higher than 650°C. Even at 600°C, only about 30 min was sufficient for the process. Formation rate can be obtained by differentiating the wt% of BaPbO$_3$ with time. The results are shown in Fig. 6. Reaction mechanism should be different in these two systems according to results shown in Fig. 6. Formation rate decreases with increasing time in BaCO$_3$–PbO system (Fig. 6(a)). There are maximum formation rates (peaks) in BaCO$_3$–PbO$_2$ system (Fig. 6(b)). The peaks shift toward shorter time when the temperature increases. Therefore, the difference in reaction

Table 2
The reaction sequence from PbO$_2$ to PbO

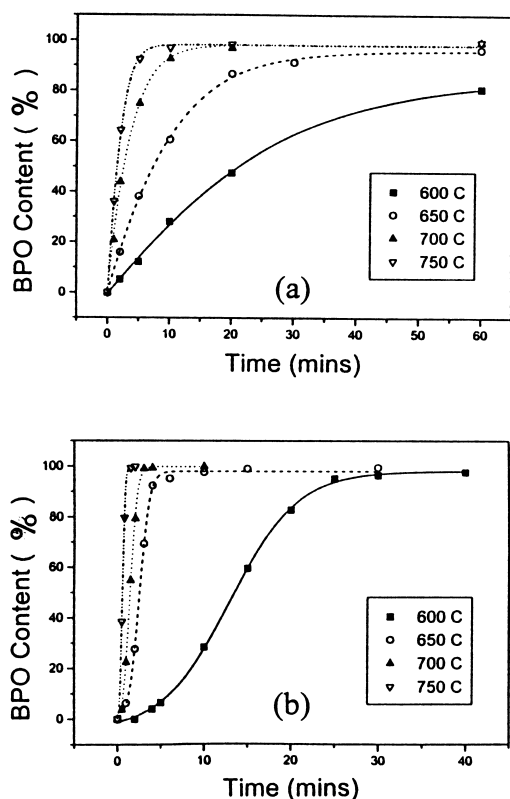| Region	Reaction	Weight loss (%) (O$_{loss}$/(BaCO$_3$+PbO$_2$))
1	PbO$_2$→PbO$_{1.57}$	1.58
2	PbO$_{1.57}$→Pb$_3$O$_4$	2.45
3	Pb$_3$O$_4$	2.45
4	Pb$_3$O$_4$→PbO	3.67

Fig. 5. Influence of calcination time on the obtained BaPbO₃ content at various temperatures in: (a) BaCO₃–PbO system and (b) BaCO₃–PbO₂ system.
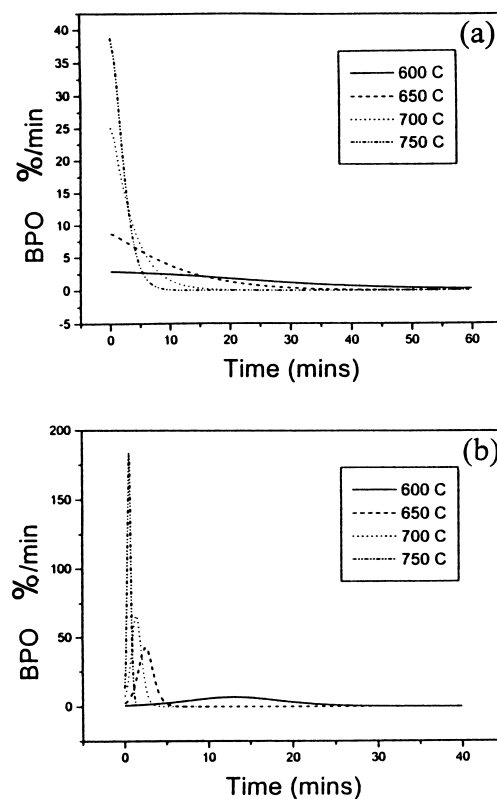

Fig. 6. Formation rate of BaPbO₃ phase as a function of temperature and time in: (a) BaCO₃–PbO system and (b) BaCO₃–PbO₂ system.

kinetics for both $BaCO_3$–PbO and $BaCO_3$–PbO_2 system is obvious.

In this investigation, the formation reaction of perovskite $BaPbO_3$ phase is heterogeneous and raw materials are multiphases. A model used to treat multiphase reaction kinetics was derived by Johnson and Mehl [19] and by Avrami [20,21]. This model was also used to analyze the $Pb[(Zn,Mg)_{1/3}Nb_{2/3}]O_3$ successfully [22]. Reaction equation is presented as follows:

$$\ln\left[\frac{1}{1-y}\right] = (kt)^n$$

where y is the formation content of $BaPbO_3$ phase; k, the reaction rate constant; t, the reaction time and n, the reaction order. Relationship of $\ln[\ln[1/(1-y)]]$ versus $\ln t$ is shown in Fig. 7, where two straight segments are found. The reaction is treated as a two-stage process and two different reaction kinetics are considered to be existent. Both $BaCO_3$–PbO and $BaCO_3$–PbO_2 systems show the same trend although the slope of each line is different. Besides, the slope of each line or the reaction order n is independent of the reaction temperature. The n value for each segment is calculated and listed in Table 3. Different n values are found in Stage 1, while they are approximately the same in Stage 2.

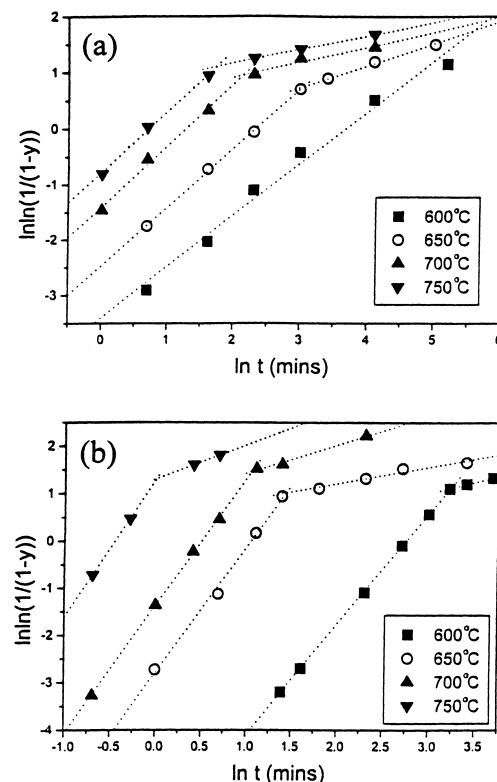The reaction rate constant k can be represented by equation

Fig. 7. Reaction kinetics fitted by the Johnson–Mehl–Avrami equation for: (a) BaCO₃–PbO system and (b) BaCO₃–PbO₂ system.

Table 3
Reaction order and activation energy of $BaPbO_3$ formation

System	Stage 1		Stage 2	
	E (kJ mol^{-1})	n	E (kJ mol^{-1})	n
$BaCO_3$–PbO	132	1	177	0.4
$BaCO_3$–PbO_2	148	5/2	169	0.5

$$k = A \exp\left(\frac{-E}{RT}\right)$$

where E is the activation energy; R, the gas constant; T, the absolute temperature and A, is a constant. Curves of $\ln k$ versus $1/T$ are plotted in Fig. 8. In the investigated temperature range, straight lines are found for both $BaCO_3$–PbO and $BaCO_3$–PbO_2 systems. The activation energies are calculated from the slopes and are shown in Table 3. The E values are higher in Stage 2 even though n values are only about 0.5 for both systems. In Stage 1, $BaCO_3$–PbO and $BaCO_3$–PbO_2 systems have n values of 1 and 5/2, respectively. This indicates that the reaction mechanisms and the controlling factors are different. According to Johnson–Mehl–Avrami model, n value of 1 means that the reaction is a surface nucleation mode [23]. The n value of 5/2 reveals that reaction is controlled by random diffusion with constant nucleation rate after the model of Marotta and Buri [24]. Therefore, reaction kinetics for both $BaCO_3$–PbO and $BaCO_3$–PbO_2
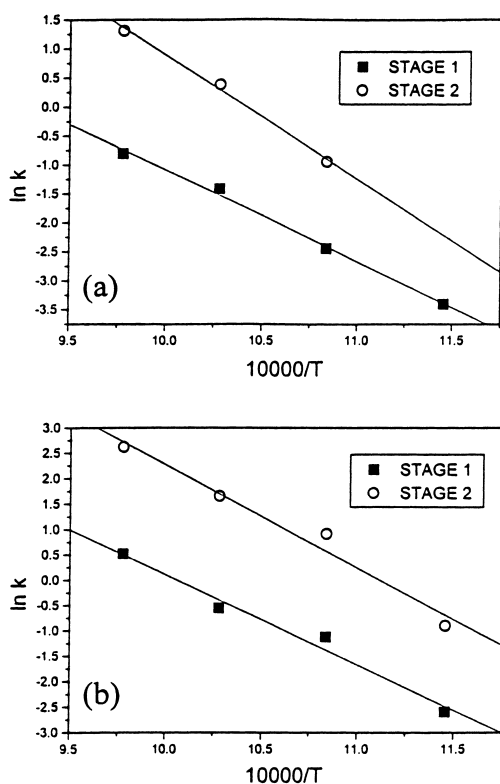
systems are controlled by different mechanisms in Stage 1. The n value of 0.5 in Stage 2 explains that the reaction is bimolecular reaction control [25]. No matter what raw materials used, reaction kinetics in Stage 2 are the same for both systems.

3.3. Mechanism of $BaPbO_3$ phase formation

The content of each raw material and $BaPbO_3$ under isothermal reaction are shown for $BaCO_3$–PbO_2 system in Fig. 9, while those for $BaCO_3$–PbO system are shown in Fig. 10. In Fig. 9(a), PbO_2 has decomposed into litharge PbO phase at 600°C. $BaPbO_3$ phase is completely formed after 25 min soaking at 600°C. PbO_2 phase disappears throughout the reaction and should take no reaction with $BaCO_3$ phase. This result is consistent with DTA/TG result shown in Fig. 3. Litharge PbO phase generally changes into massicot phase at temperatures higher than 500°C. However, no massicot PbO phase was found in $BaCO_3$–PbO_2 system. Litharge PbO phase exists even at temperature as high as 750°C, which is quite different from that of $BaCO_3$–PbO system (Fig. 10). It is believed that the litharge PbO phase causes different reaction kinetics as mentioned above. Comparing with Fig. 3(b), weight loss of $BaCO_3$ phase occurs continuously before the formation of $BaPbO_3$ phase. That means $BaCO_3$ changes into BaO by releasing CO_2. XRD analysis, which shows no BaO phase detected, indicates that the introduction of BaO into PbO litharge phase to form an intermediate solid solution phase (Pb,Ba)O is very possible. This may also explain why litharge PbO phase can be found
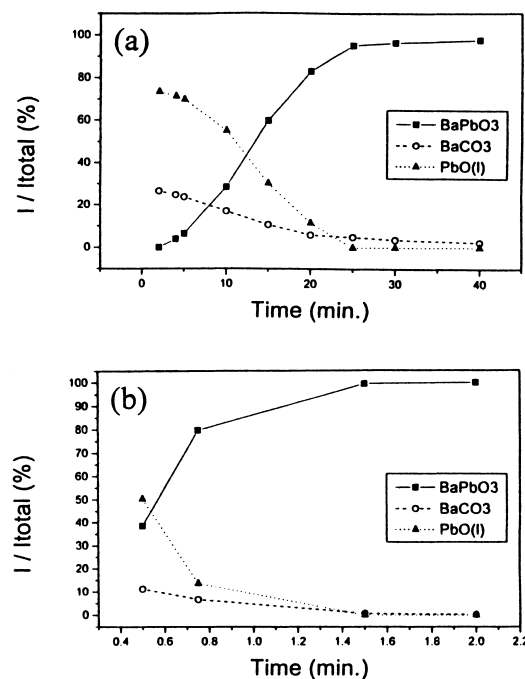

Fig. 8. Activation energy of $BaPbO_3$ formation in: (a) $BaCO_3$–PbO system and (b) $BaCO_3$–PbO_2 system derived by fitting to the Arrhenius equation.

Fig. 9. The amounts of $BaPbO_3$ and raw materials as a function of time at: (a) 600°C and (b) 750°C in $BaCO_3$–PbO_2 system.
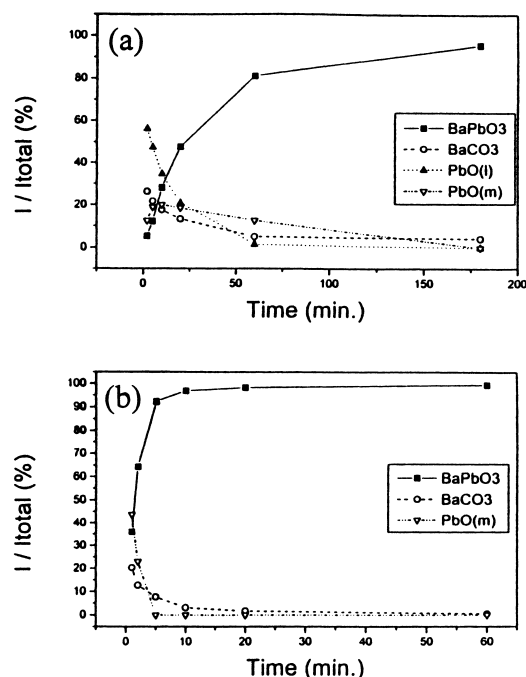
Fig. 10. The amounts of $BaPbO_3$ and raw materials as a function of time at: (a) 600°C and (b) 750°C in $BaCO_3$–PbO system.

at high temperature. The $BaPbO_3$ phase is nucleated from the solid solution phase through the dissolving BaO.
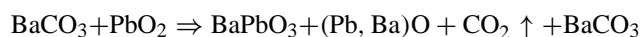
In $BaCO_3$–PbO system, Fig. 10(a) shows that litharge PbO phase coexists with massicot PbO phase at 600°C while Fig. 10(b) shows that at 750°C litharge PbO phase changes completely into massicot PbO phase. The content of massicot PbO phase increases with the PbO transformation from litharge and decreases with the $BaPbO_3$ phase formation. This explains that massicot PbO phase increases initially then decreases afterward (Fig. 10(a)). Phase transformation proceeds sharply at temperature 750°C as seen in Fig. 10(b). According to the results, $BaPbO_3$ phase is formed by reaction of $BaCO_3$ and massicot PbO phase directly. No litharge solid solution was found in $BaCO_3$–PbO system.

According to the data listed in Table 3, both $BaCO_3$–PbO and $BaCO_3$–PbO_2 present a two-stage reaction with the same reaction order at second stage. In Stage 2, $BaPbO_3$ and $BaCO_3$ are main phases as shown in Figs. 9 and 10. The incorporation of BaO into $BaPbO_3$ dominates reaction in this stage. Consequently, both systems present the same behavior in Stage 2.
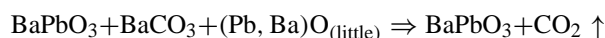
The overall reaction of $BaPbO_3$ phase formation can be presented as follows.
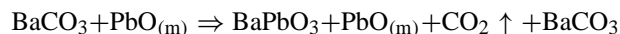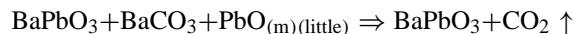
In $BaCO_3$–PbO_2 system:

Stage 1 ($n=5/2$)

$$BaCO_3 + PbO_2 \Rightarrow BaPbO_3 + (Pb, Ba)O + CO_2 \uparrow + BaCO_3$$

Stage 2 ($n=0.5$)

$$BaPbO_3 + BaCO_3 + (Pb, Ba)O_{(little)} \Rightarrow BaPbO_3 + CO_2 \uparrow$$

In $BaCO_3$–PbO system:

Stage 1 ($n=1$)

$$BaCO_3 + PbO_{(m)} \Rightarrow BaPbO_3 + PbO_{(m)} + CO_2 \uparrow + BaCO_3$$

Stage 2 ($n=0.4$)

$$BaPbO_3 + BaCO_3 + PbO_{(m)(little)} \Rightarrow BaPbO_3 + CO_2 \uparrow$$

4. Conclusions

Reaction kinetics and formation mechanisms of $BaPbO_3$ are different in $BaCO_3$–PbO and $BaCO_3$–PbO_2 systems. The intermediate phases of solid solution litharge and massicot PbO phase play a main role in the $BaPbO_3$ formation in $BaCO_3$–PbO_2 and $BaCO_3$–PbO systems, respectively. In the $BaCO_3$–PbO system, surface nucleation model with reaction order $n=1$ and activation energy $E=132\,kJ\,mol^{-1}$ was found for the first reaction stage. The diffusion controlled crystal growth with $n=5/2$ and $E=148\,kJ\,mol^{-1}$ was proposed in the first reaction stage for the $BaCO_3$–PbO_2 system. In the second reaction stage, both systems show similar reaction behavior and the bimolecular reaction is the dominant mechanism.

References

[1] R.D. Shannon, P.E. Bierstedt, J. Am. Ceram. Soc. 53 (1970) 635.
[2] S. Takahashi, S. Yoneda, H. Shimooka, M. Kuwabara, J. Ceram. Soc. Jpn. 103 (1995) 660, (in japanes).
[3] A.W. Sleight, J.L. Gillson, P.E. Bierstedt, Solid State Comm. 17 (1975) 27.
[4] T.M. Rice, L. Sneddon, Phys. Rev. Lett. 47 (1981) 689.
[5] A. Batlogg, Physica B 126 (1984) 275.
[6] K. Kitazawa, S. Uchida, S. Tanaka, Physica B 135 (1985) 505.
[7] Y. Enomoto, M. Suzuki, T. Murakami, T. Inukai, T. Inamura, Jpn. J. Appl. Phys. 20 (1981) L661.
[8] Y. Enomoto, M. Suzuki, T. Murakami, T. Inamura, Jpn. J. Appl. Phys. 21 (1982) L384.
[9] M. Ito, Y. Enomoto, M. Suzuki, T. Murakami, T. Inamura, Jpn. J. Appl. Phys. 21 (1982) L375.
[10] M. Ito, Y. Enomoto, T. Murakami, Appl. Phys. Lett. 43 (1983) 314.
[11] D. Greninger, V. Kollonitsch, C.H. Kline, Lead Chemicals, New York, 1974, (Chapter 1).
[12] B. Dickens, J. Inorg. Nucl. Chem. 27 (1965) 1503.
[13] B. Dickens, J. Inorg. Nucl. Chem. 27 (1965) 1495.
[14] W.B. White, F. Dachille, R. Roy, J. Am. Ceram. Soc. 44 (1961) 170.
[15] M. Senna, H. Kuno, J. Am. Ceram. Soc 54 (1971) 259.
[16] D. Lewis, K.O. Northwood, R.C. Reeve, J. Appl. Crystallogr. 2 (1969) 156.
[17] E.W. Abel, Lead in Comprehensive Inorganic Chemistry, Oxford, UK, 1973, pp. 105–146.
[18] H.P. Klug, L.E. Alexander, X-ray Diffraction Procedures for Polycrystalline and Amorphous Materials, Wiley, New York, 1974.
[19] W.A. Johnson, R.F. Mehl, Trans. AIME 135 (1939) 416.
[20] M. Avrami, J. Chem. Phys. 7 (1939) 1103.
[21] M. Avrami, J. Chem. Phys. 9 (1941) 177.
[22] S.Y. Chen, C.M. Wang, S.Y. Cheng, J. Am. Ceram. Soc. 74 (1991) 2506.
[23] K. Marotta, S. Sakka, J. Non-Cryst. Solids 38/39 (1980) 741.
[24] A. Marotta, A. Buri, Thermochim. Acta 25 (1978) 155.
[25] J. Sestak, G. Berggren, Thermochim. Acta 3 (1971) 1.